ARTICLES

Solvation Dynamics of Coumarin 153 in Alcohols Confined in Silica Nanochannels

Toshio Kamijo,[†] Akira Yamaguchi,[†] Shintaro Suzuki,[†] Norio Teramae,[†,*] Tetsuji Itoh,[‡] and Takuji Ikeda[‡]

Department of Chemistry, Graduate School of Science, Tohoku University, Aoba-ku, Sendai 980-8578, Japan, and Research Center for Compact Chemical Process, National Institute of Advanced Industrial Science and Technology (AIST), Nigatake 4-2-1, Miyagino-ku, Sendai 983-8551, Japan

Received: April 22, 2008; Revised Manuscript Received: August 27, 2008

Solvation dynamics in alcohols confined in silica nanochannels was examined by time-resolved fluorescence spectroscopy using coumarin 153 (C153) as a fluorescent probe. Surfactant-templated mesoporous silica was fabricated inside the pores of an anodic alumina membrane. The surfactant was removed by calcination to give mesoporous silica (Cal-NAM) containing one-dimensional (1D) silica nanochannels (diameter, 3.1 nm) whose inner surface was covered with silanol groups. By treating Cal-NAM with trimethylchlorosilane, trimethylsilyl (TMS) groups were formed on the inner surface of the silica nanochannels (TMS-NAM). Fluorescence dynamic Stokes shifts of C153 were measured in alcohols (ethanol, butanol, hexanol, and decanol) confined in the silica nanochannels of Cal- and TMS-NAMs, and the time-dependent fluorescence decay profiles could be best fitted by a biexponential function. The estimated solvent relaxation times were much larger than those observed in bulk alcohols for both Cal- and TMS-NAMs when ethanol or butanol was used as a solvent, indicating that the mobility of these alcohol molecules was restricted within the silica nanochannels. However, hexanol or decanol in Cal- and TMS-NAMs did not cause a remarkable increase in the solvent relaxation time in contrast to ethanol or butanol. Therefore, it was concluded that a relatively rigid assembly of alcohols (an alcohol chain) was formed within the silica nanochannels by hydrogen bonding interaction and van der Waals force between the surface functional groups of the silica nanochannels and alcohol molecules and by the successive interaction between alcohol molecules when alcohol with a short alkyl chain (ethanol or butanol) was used as a solvent.

1. Introduction

Surfactant-templated mesoporous silica holds promise as a nanomaterial applicable to various fields due to its inherently desirable properties such as high surface area and large adsorption capacity. These characteristic properties allow mesoporous silica to be used as sorbents and catalysts with high efficiency.[1−4] Mesoporous silica has a uniform pore diameter of molecular dimensions, and this characteristic can be utilized for size-exclusive separation.[5−8] The uniform pore can also work as a template for fabricating organic and inorganic nanomaterials.[9−12] Moreover, extensive studies have been reported on incorporating functional groups into silica mesopores to develop a functional mesoporous silica.[13−18]

Diffusivity of an organic solute molecule within porous materials is an important subject to be understood because diffusivity is related to various chemical processes. It has been quantitatively examined by several techniques.[19−23] Fu et al.[21] applied single-molecule fluorescence correlation spectroscopy to estimate an apparent diffusion coefficient of Nile Red in a thin film of surfactant-templated mesoporous silica, and they found that the diffusion coefficient was on the order of 10^{-10} cm^2 s^{-1}. Nakatani's group[19] studied the diffusivities of organic dye molecules within porous silica gels by microcapillary manipulation injection and microabsorption methods, and they estimated diffusion coefficients were on the order of 10^{-9} to 10^{-10} cm^2 s^{-1}. Since the diffusion coefficient of small organic molecules in aqueous and organic media has been reported to be on the order of 10^{-6} cm^2 s^{-1},[24,25] the diffusion coefficients of organic molecules in porous materials must be smaller than those in a bulk solution phase. These small diffusion coefficients have often been explained by adsorption of solute and/or solvent molecules on the inner pore wall.[21] On the other hand, several studies have examined the effect of solvent properties on the diffusivity of solute molecules confined in the mesopores. For example, in our previous study, the apparent diffusion coefficient of tris(2,2′-bipyridyl)ruthenium(II) in ethanol confined in mesoporous silica whose pore surface had been modified by alkylsilanes ($(CH_3)_3-Si$ and C_4H_9 $(CH_3)_2-Si$) was found to be on the order of 10^{-10} cm^2 s^{-1}.[22] Since the diffusion coefficient was smaller for protic solvents (methanol and ethanol) than for aprotic solvents (acetonitrile and dimethyl sulfoxide (DMSO)), it was inferred that the hydrogen bonding interaction between alcohol molecules confined in the pores was responsible for the slow diffusivity of tris(2,2′-bipyridyl)ruthenium(II). Takahashi et al.[20] examined the diffusion coefficients of ketones in alkanes with different chain lengths confined in porous sol−gel glasses with different pore sizes and found the diffusivity of ketones

* To whom correspondence should be addressed. Fax: +81-22-795-6552. E-mail: teramae@mail.tains. tohoku.ac.jp.
† Tohoku University.
‡ AIST.

10.1021/jp8034743 CCC: $40.75
Published on Web 10/23/2008

CHART 1: Coumarin 153 (C153)

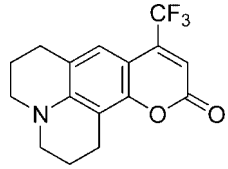

in mesopores (4.0 and 10.5 nm) decreased with increasing molecular size of solvents, and the diffusivity in small mesopores (4.0 nm) was larger for solvents with an odd number of carbon atoms than for those with an even number of carbon atoms. These results suggest that an assembly of solvent molecules might be formed within small-sized mesopores and that the rigidity of the assembly determines the diffusivity of solute molecules.

As a spectroscopic approach for examining the rigidity of media, solvation dynamics offers valuable information since solvation dynamics is affected by the mobility and viscosity of media surrounding a fluorescent probe molecule.[26−32] Several studies have been reported on solvation dynamics in various porous silica materials, including porous sol−gel silica matrcies,[27−29] a porous sol−gel silica matrix in the presence of surfactant[30] or phospholipids,[31] and a mesostructured silica with cetyltrimethylammonium bromide (CTAB).[32] In these studies, water or ethanol was used as the solvent confined in the silica mesopores. In this study, we examine the solvation dynamics using a series of alcohols (ethanol, butanol, hexanol, and decanol) confined in the pores of mesoporous silica by measuring the time-dependent fluorescence spectral shift (dynamic Stokes shift) using coumarin 153 (C153) as a fluorescent probe. The chemical structure of C153 is shown in Chart 1. Mesoporous silica materials were synthesized according to our previous papers,[7,8] and surfactant-templated mesoporous silica was formed inside the columnar pores of an anodic alumina membrane which is hereafter referred to as the nanochannel-incorporated alumina membrane (NAM). As shown in Figure 1, the mesoporous silica is composed of the silica nanochannels with perpendicular orientation to the membrane surface. We used two different NAMs; one is the calcined NAM (Cal-NAM) in which silanol groups cover the inner channel surface, and the other is the modified NAM (TMS-NAM) in which trimethylsilyl (TMS) groups cover the inner channel surface. In the previous studies on reorientational dynamics and solvation dynamics of liquids in porous silica glasses,[28,29] dichlorodimethylsilane was used for the modification of the inner surface of the pores. In this study, TMS was chosen as the surface modifier because the TMS groups can form a closely packed monolayer on the silica surface without polycondensation which often occurs if dichlorodimethylsilane is used. The structures and surface conditions of the prepared NAMs were characterized by measurements of nitrogen adsorption/desorption isotherms and ^{29}Si-CP/MAS NMR. From the dynamic Stokes shift of C153 in alcohols confined in the pores of these NAMs, we discuss the effect of the surface functional group (silanol or TMS) and the size of alcohols on the rigidity of alcohols confined in the silica nanochannels.

2. Experimental Section

2.1. Materials. Trimethylchlorosilane (TMCS) was purchased from Azmax Inc. (Chiba, Japan). CTAB was purchased from Tokyo Chemical Industries, Ltd. (Tokyo, Japan). Other reagents used for synthesis and modification of NAM were purchased from Wako Pure Chemical Industries, Ltd. (Osaka, Japan).

C153 was purchased from Sigma-Aldrich Japan (Tokyo, Japan) and used as received. Ethanol and butanol of spectroscopical reagent grade were purchased from Nacalai Tesque, Inc. (Tokyo, Japan). Hexanol and decanol of analytical reagent grade were purchased from Sigma-Aldrich Japan. Water contents of alcohols were determined by the Karl Fischer method and were 0.18 mol % for ethanol, 0.069 mol % for butanol, 0.071 mol % for hexanol, and 0.11 mol % for decanol.

2.2. Preparation and Characterization of NAMs. The details of the preparation procedures of NAM were described previously.[7] In brief, an anodic alumina membrane with an average pore diameter of 200 nm (Whatman International Ltd., Maidstone, England) was placed in an ordinary membrane filtration apparatus. An acidic precursor solution containing CTAB and tetraethyl orthosilicate (TEOS) was dropped onto the anodic alumina membrane while moderate aspiration was applied, so that the precursor solution penetrated into the columnar alumina pores. The alumina membrane incorporating the precursor solution was then dried in air at room temperature. In this way, an assembly of silica−surfactant nanochannels was formed inside each columnar alumina pore and NAM was obtained. Subsequently, NAM was calcined at 600 °C for 2 h to remove the surfactant-template. Hereafter, we designate the calcined NAM as Cal-NAM.

The inner surface of the silica nanochannels of Cal-NAM was modified by TMCS according to the literature[22,33,34] with some modifications. Cal-NAMs were immersed in a mixture of 9 mL of dry toluene and 1 mL of TMCS, and the mixed solution was refluxed at 70 °C for 24 h. Then, dry ethanol was added to deactivate TMCS remaining in the mixed solution. The modified NAMs thus prepared were rinsed with toluene and acetone three times each. Finally, the modified NAMs were dried under vacuum for 2 h at 90 °C. Hereafter, we designate the Cal-NAM modified by TMCS as TMS-NAM.

^{29}Si CP/MAS NMR spectra were recorded on a Bruker AVANCE 400WB spectrometer using a double air bearing CP/MAS DVT probe head with 7 mm ZrO_2 rotors. The spinning speed was 5 kHz. Nitrogen adsorption−desorption isotherms were measured on a Micrometric ASAP 2020 instrument. The specific surface areas of Cal- and TMS-NAMs were calculated using the multiple-point Brunauer−Emmett−Teller (BET) method, and the pore size distribution was calculated from the adsorption branch of the isotherms using the Barrett−Joyner−Halenda (BJH) method. Yanaco model CHN MT-6 elemental analyzer was used to determine the carbon and nitrogen weight percentages in TMS-NAM and Yanaco model HNS-15/HSU-20 halogen and sulfur analyzer was used to determine the halogen weight percentage.

2.3. Fluorescence Measurements. To prepare NAM samples for fluorescence measurements, Cal-NAM or TMS-NAM was immersed in an alcohol solution of C153 (10 mM). After applying ultrasonication for 5 min, each NAM sample was kept overnight in the same alcohol solution to distribute C153 and alcohol into the silica nanochannels. Subsequently, the NAM sample was rinsed with pure alcohol and then was set in a measuring cell. Rinsing of the NAM sample was done in a glovebox under the saturated alcohol vapor condition, and the saturated alcohol vapor condition was also kept during the fluorescence measurements. The concentrations of C153 inside the sample membrane was estimated, and they were less than 9×10^{-9} mol per each membrane (see Supporting Information). This concentration means that the occupied space of a single C153 molecule inside the silica nanochannel is larger than 534

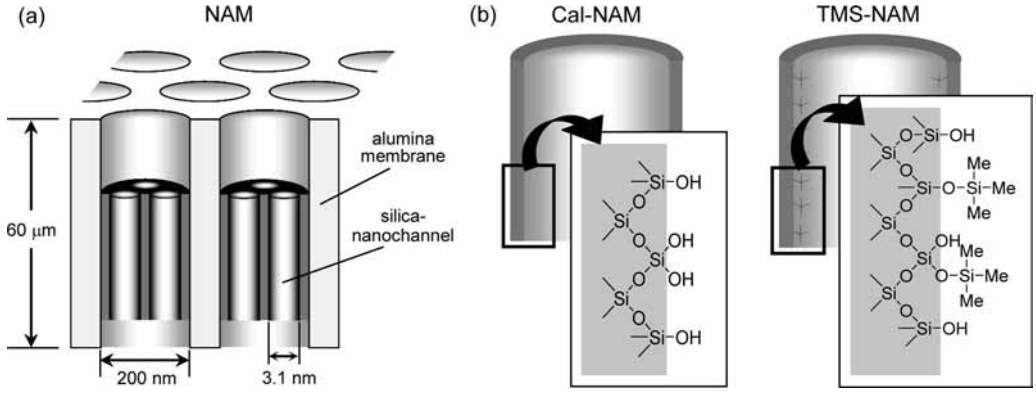

Figure 1. Schematic illustration of (a) the silica nanochannels (channel diameter = 3.1 nm) formed inside the columnar alumina pore (pore diameter = ca. 200 nm) and (b) the mesostructure of the silica nanochannels (Cal-NAM, TMS-NAM).

nm^3/molecule, suggesting that C153 is monodispersed inside the silica nanochannel.

Steady-state fluorescence spectra of C153 were measured by using a violet continuous-wave (CW) diode laser (Oxxius, model 405-50-COL-004; wavelength, 409 nm) as an excitation source and a photonic multichannel analyzer (Hamamatsu, model C-5633-31) as a detector.

The experimental setup for time-resolved fluorescence spectroscopy was described in detail previously.[32,35] The measurement system was composed of a mode-locked titanium:sapphire laser (Spectra-Physics, Tsunami 3960; ca. 100 fs at 770 nm, 82 MHz) pumped by a CW visible laser (Spectra-Physics, Millennia-Pro), a polychromator (Hamamatsu, C5094), and a streak scope (Hamamatsu, C4334). The repetition rate of the titanium: sapphire laser was reduced to 4 MHz using an electrooptic modulator (Spectra-Physics, Model 3980), and the second harmonic of the Ti:sapphire laser generated by an LBO crystal (Spectra-Physics, GWU) was used as an excitation source. The excitation laser beam was shone on a NAM sample in a quartz cuvette (25 mm × 25 mm), and fluorescence from the NAM sample was focused on the slit of the polychromator. The instrumental time resolution of the present system was approximately 50 ps at 2 ns full scale, 100 ps at 5 ns full scale, and 170 ps at 10 ns full scale. The maximum fluorescence wavelengths were estimated by fitting time-resolved spectra to a log-normal function.[26,36]

3. Results

3.1. Characterization of Cal-NAM and TMS-NAM. N_2 adsorption isotherms of Cal- and TMS-NAMs are shown in Figure 2, and the inset shows the pore size distribution curves calculated by the BJH method.[37] The inflection position in the relative pressure (p/p_0; p and p_0 denote the adsorbate pressure and adsorbate saturated pressure, respectively) is similar to that found in CTAB-templated MCM-41.[38] The structural parameters deduced from the isotherms are summarized in Table 1. The pore diameter for Cal-NAM is estimated as 3.1 nm which represents the diameter of silica nanochannels formed inside the pores of an anodic alumina membrane, since the estimated diameter agrees well with our previous result (3.4 ± 0.2 nm)[7] obtained for CTAB-templated mesoporous silica. The BET surface area and average channel diameter of TMS-NAM are slightly smaller than those of Cal-NAM (Table 1), which is ascribed to the formation of the TMS layer on the inner surface of the silica nanochannels.

In the elemental analysis of TMS-NAM, nitrogen and chloride are not detected at all, indicating that the template surfactant and unreacted TMCS were sufficiently removed from TMS-NAM. The carbon content derived from the elemental analysis is used for the estimation of the surface density of the TMS group immobilized on the inner surface of the silica nanochannels. The details of the estimation procedure were described in our previous paper,[22] and the estimated value is 2.1 molecules/nm^2. The surface density of the TMS group has been studied by many researchers and is reported as 2.1−2.7 molecules/nm^2 at the maximum density.[22,39−42] Hence, the surface coverage of the TMS group in TMS-NAM can be estimated as 0.8−1.0, indicating that TMS groups are packed closely together to form the TMS layer on the inner surface of the silica nanochannels. The density of the surface silanol groups of the surfactant-templated mesoporous silica prepared by an acidic precursor was reported as 3−4 groups/nm^2.[43] From the surface densities of the TMS and silanol groups, we conclude that at least half to two-thirds of the surface silanol groups were modified by the TMS groups.

The TMS groups of TMS-NAM were further examined by NMR. Figure 3 shows ^{29}Si CP/MAS NMR spectra of Cal- and

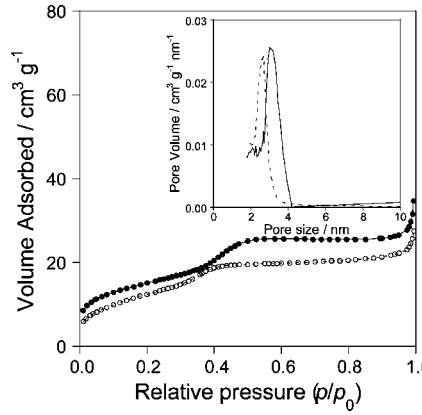

Figure 2. Nitrogen adsorption isotherms of Cal-NAM (●) and TMS-NAM (○). The inset shows the pore size distribution curves for Cal-NAM (solid line) and TMS-NAM (dashed line).

TABLE 1: Structural Parameters of Cal-NAM and TMS-NAM

system	BET surface area [a]/ (m^2 g^{-1})	BJH pore diameter[a]/ nm	carbon content[b]/%	surface density/ (molecules nm^{-2})
Cal-NAM	53.5	3.1		
TMS-NAM	46.3	2.6	0.637	2.1

[a] These values are derived from the nitrogen adsorption and desorption isotherms of Cal-NAM and TMS-NAM after calcination. [b] Results of elemental analysis.

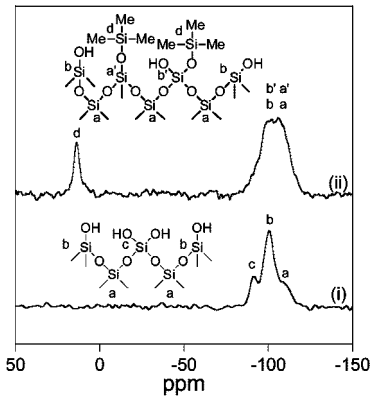

Figure 3. ^{29}Si CP/MAS NMR spectra for (i) Cal-NAM and (ii) TMS-NAM.

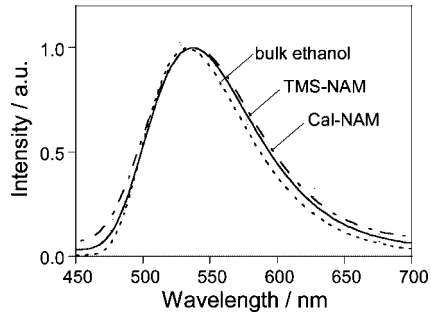

Figure 4. Fluorescence spectra of C153 in bulk ethanol (dotted line), Cal-NAM (dashed line), and TMS-NAM (solid line).

TABLE 2: Maximum Wavelength (nm) of Fluorescence Spectra of C153 in Bulk, Cal-NAM, and TMS-NAM

system	ethanol	butanol	hexanol	decanol
bulk	533	527	526	519
Cal-NAM	538[a]	532	527	532
TMS-NAM	537	529	525	526

[a] The standard deviation of the maximum wavelength is 2 nm for Cal-NAM (ethanol) by the four independent measurements.

TMS-NAMs together with the assignment of each resonant peak. As shown in spectrum i in Figure 3, Cal-NAM gives three resonances at −110, −101, and −91 ppm, and these resonances can be assigned to the silicon sites (*Si) of (a) Q^4, *Si(OSi)$_4$, (b) Q^3, HO*Si(OSi)$_3$, and (c) Q^2, (HO)$_2$*Si(OSi)$_2$, respectively, according to the literature.[34] The Q^3 site is associated with the isolated silanol group, and the Q^2 site with the geminal silanol group. In contrast to Cal-NAM, TMS-NAM gives a sharp peak at 14 ppm due to the silicon site of a TMS group,[34] and the intensity of the Q^4 silicon (a + a′) increases, whereas the intensity of the Q^2 silicon (c) decreases, as shown in spectrum i in Figure 3. These changes in the intensity can be ascribed to the reduction of the isolated and geminal silanol groups by immobilizing the TMS groups on the inner surface of the silica nanochannels.

3.2. Steady-State Fluorescence Spectra. Figure 4 shows fluorescence spectra of C153 in bulk ethanol, Cal-NAM, and TMS-NAM. Fluorescence spectra were also measured using butanol, hexanol, and decanol as a solvent, and the results are shown in Figure S3 of the Supporting Information. Maximum fluorescence wavelengths of C153 are summarized in Table 2. As seen in the table, there is a tendency that the fluorescence maximum of C153 in Cal-NAM and TMS-NAM is slightly red-shifted compared to bulk alcohols. Since the maximum wavelength of the fluorescence spectrum of C153 reflects the polarity of the medium surrounding C153,[26,44] the slight red-shift indicates that C153 molecules are incorporated into the silica nanochannels and TMS-modified silica nanochannels where the polarity is slightly higher than the bulk phase.

3.3. Time-Resolved Fluorescence Spectra. The wavelength-dependent fluorescence decay curves of C153 were measured in bulk ethanol as well as in Cal- and TMS-NAMs where ethanol is confined in the silica nanochannels and TMS-modified silica nanochannels, by dividing the fluorescence spectral region into three, that is, (a) short (490−500 nm), (b) middle (525−535 nm), and (c) long (600−630 nm) wavelength regions. The results are shown in Figure 5. In all samples, C153 exhibits wavelength-dependent fluorescence decay profiles. The time-resolved fluorescence response shows a fast decay in the short-wavelength region (Figure 5a), and the response becomes slower in the middle-wavelength region (Figure 5b). Both rise and decay components appear in the long-wavelength region (Figure 5c). Similar wavelength-dependent fluorescence decay profiles are observed for C153 in both bulk and NAMs when other alcohols were used as a solvent. From the observed time-resolved fluorescence response, we constructed the time-resolved fluorescence spectra according to the literature.[32,45]

Figure 6 (top panels) shows time-resolved fluorescence spectra of C153 in bulk ethanol and in confined ethanol within silica nanochannels and TMS-modified silica nanochannels. The time-dependent Stokes shift can be easily recognized in all spectra. Time-dependent fluorescence spectra were quantitatively analyzed using a time-correlation function, $C(t)$, which is defined by[26]

$$C(t) = \frac{\nu(t) - \nu(\infty)}{\nu(0) - \nu(\infty)} \tag{1}$$

where $\nu(0)$, $\nu(t)$, and $\nu(\infty)$ are the maximum fluorescence frequencies at times 0, t, and ∞, respectively. The decay of $C(t)$ is shown in Figure 6 (bottom row of panels). The observed decay profiles, $\nu(t)$, can be fitted by a biexponential function given by

$$C(t) = a_1 \exp\left(-\frac{t}{\tau_1}\right) + a_2 \exp\left(-\frac{t}{\tau_2}\right) \tag{2}$$

where τ_1 and τ_2 are the solvent relaxation times, and a_1 and a_2 are their amplitudes. The average relaxation time $\langle\tau_s\rangle$ is given by[32,35]

$$\langle\tau_s\rangle = a_1\tau_1 + a_2\tau_2 \tag{3}$$

The decay parameters are summarized in Table 3. The time-dependent Stokes shifts were observed for other alcohols, and those results are shown in Figure S4 of the Supporting Information, while the decay parameters are also listed in Table 3.

As seen in Table 3, the average relaxation times found for Cal- and TMS-NAMs are longer than that for bulk alcohols. In the following discussion, we define the average relaxation times found for Cal-NAM, TMS-NAM, and bulk alcohols as $\langle\tau_s\rangle_{\text{Cal-NAM}}$, $\langle\tau_s\rangle_{\text{TMS-NAM}}$, and $\langle\tau_s\rangle_{\text{bulk}}$, respectively. Figure 7 shows the ratios of $\langle\tau_s\rangle_{\text{Cal-NAM}}$ to $\langle\tau_s\rangle_{\text{bulk}}$ and of $\langle\tau_s\rangle_{\text{TMS-NAM}}$ to $\langle\tau_s\rangle_{\text{bulk}}$ against the length of alkyl chain of alcohols used as a solvent.

Solvation dynamics has been extensively studied to date, and it is well-known that an initial ultrafast decay (1−10 ps or less) and the subsequent decay components contribute to the observed solvation dynamics. Thus, it should be noted that an ultrafast component of the dynamic Stokes shift that occurs within our instrumental time resolution was not observed in the present study.

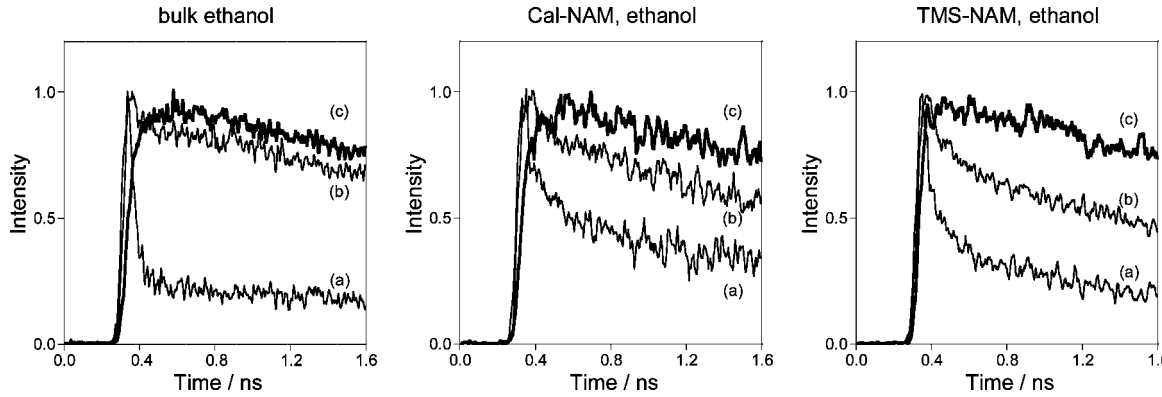

Figure 5. Fluorescence decay profiles of C153 in bulk ethanol and in ethanol confined to NAM for different wavelength regions: (a) 490−500, (b) 525−535, and (c) 600−630 nm. All decay profiles were measured by a streak scope at 2 ns full scale.

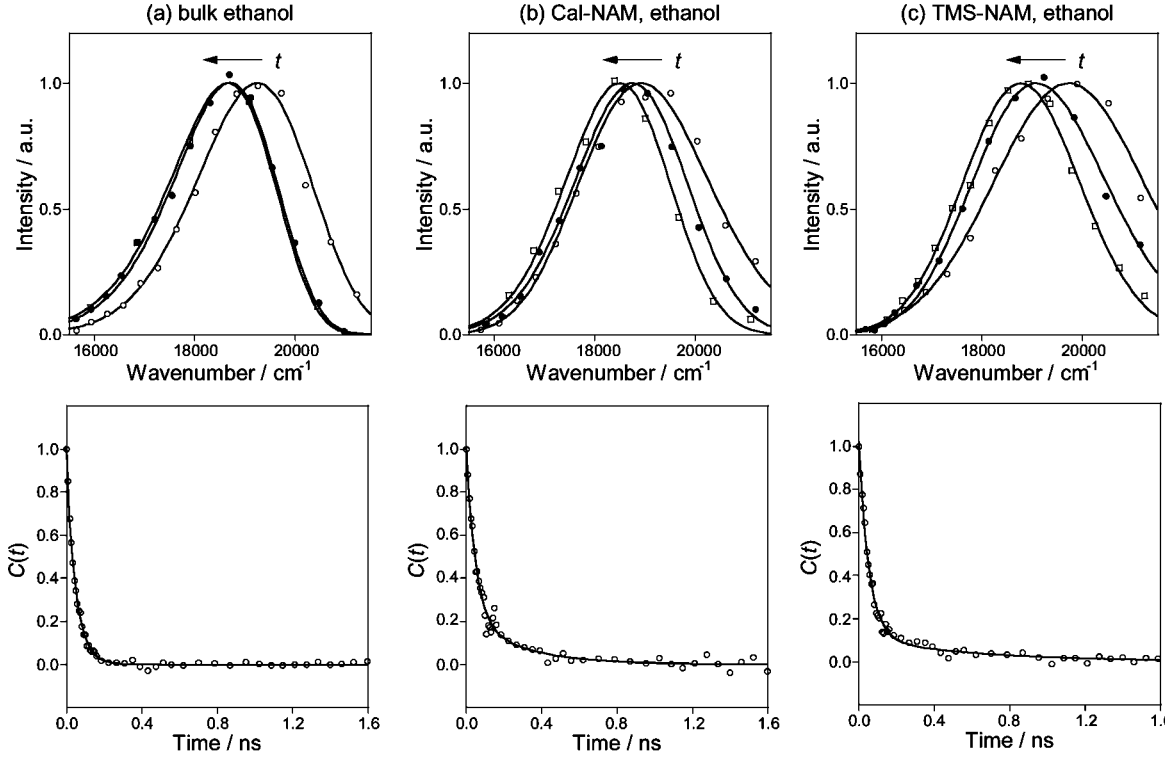

Figure 6. Time-resolved fluorescence spectra of coumarin 153 in (a) bulk, (b) Cal-NAM, and (c) TMS-NAM (upper row) and decays of the time-correlation function (bottom row). Time-resolved fluorescence spectra at 0 (○), 0.1 (●), and 1.5 ns (□) are shown in the upper row of panels. The solid lines in the upper row of the panels denote the best fit to a log-normal line shape function. The solid lines in the bottom row of panels denote the best fit to a biexponential function.

4. Discussion

4.1. Solvation Dynamics in Cal- and TMS-NAMs. In the wavelength-dependent fluorescence decay curves of C153 shown in Figure 5, a fast decay is observed in the short-wavelength region (Figure 5a) and the decay becomes slower in the middle-wavelength region (Figure 5b). Both rise and decay are observed in the long-wavelength region (Figure 5c). Such behavior can be ascribed to a continuous time-dependent spectral shift rather than kinetics involving a few discrete excited states.[45] Accordingly, the dynamic Stokes shift observed in the constructed time-resolved fluorescence spectra (Figure 6) can be ascribed to the solvation dynamics caused by alcohol molecules. As listed in Table 3, the average solvent relaxation time $\langle\tau_s\rangle$ in bulk ethanol is 47 ps with ±20% fitting error and this value is larger than the reported value (ca. 16 ps) obtained by the fluorescence up-conversion measurement.[29] The frequency shift of the dynamic Stokes shift for bulk ethanol (Figure 6a) is about three times smaller than that measured by Horng et al.[44] and is about two times smaller than that by Baumann et al.[29] The smaller frequency shift observed in this study may be ascribed to the inferior time resolution of our measurement system (50 ps at 2 ns full scale) compared with the measurement system used in the literature (better than 400 fs),[29,44] and the ultrafast dynamics that may be responsible for a considerable part of the solvation dynamics could not be observed in this study. Accordingly, in the following discussion on the solvation dynamics, we focus on the average relaxation time without considering each component of the relaxation times.

The average relaxation times observed for ethanol in Cal-NAM and TMS-NAM are 100 and 123 ps, respectively (Table 3), and these values are much larger than that in bulk ethanol (47 ps). The slow solvent relaxation time of C153 might be ascribed to the characteristics of ethanol confined in the silica nanochannels of Cal- and TMS-NAMs.

As another possible cause of the slow solvent relaxation time other than the confinement of ethanol, the contribution of water

TABLE 3: Decay Parameters of $C(t)$ for Bulk, Cal-NAM, and TMS-NAM

system	$\Delta\nu^a$/ cm^{-1}	a_1	$\tau_1{}^b$/ ps	a_2	$\tau_2{}^b$/ ps	$\langle\tau_s\rangle^c$/ ps
ethanol						
bulk	594	0.14	18	0.86	52	47
Cal-NAM	593	0.78	49	0.22	283	100
TMS-NAM	682	0.73	53	0.27	308	123
butanol						
bulk	1031	0.73	81	0.27	135	96
Cal-NAM	1152	0.75	88	0.25	712	244
TMS-NAM	913	0.76	102	0.24	802	272
hexanol						
bulk	1144	0.79	131	0.21	430	192
Cal-NAM	932	0.80	120	0.20	674	231
TMS-NAM	1061	0.61	137	0.39	447	257
decanol						
bulk	1559	0.60	236	0.40	850	480
Cal-NAM	680	0.57	167	0.43	1009	531
TMS-NAM	1318	0.37	110	0.63	843	573

[a] ± 50 cm^{-1}. [b] $\pm 15\%$. [c] $\pm 20\%$.

molecules in ethanol (0.18 mol % determined by the Karl Fischer method) to the solvation dynamics can be considered. However, this possibility can be excluded by considering the solvent relaxation times of C153 in Cal- and TMS-NAMs. Water molecules are considered to bind to surface silanol groups of silica nanochannels of Cal-NAM, whereas hydrophobic TMS groups of TMS-NAM cannot interact with water molecules. In our previous study of solvation dynamics of a coumarin dye immobilized on a hydrophilic mica surface, the coumarin dye exhibited slow solvation dynamics in an ethanol−water mixture.[46] This slow solvation dynamics was ascribed to a rigid hydrogen bonding network of water molecules on the mica surface.[46] According to this result, solvation dynamics must be slower in Cal-NAM compared to TMS-NAM. However, the solvent relaxation times are nearly comparable for both Cal-NAM (100 ps) and TMS-NAM (123 ps) within the experimental error ($\pm 20\%$). Accordingly, we can disregard the contribution of water molecules to the slow solvation dynamics of C153.

As for solvation dynamics in porous materials, Baumann et al.[28,29] proposed two models, that is, the enhanced polarization field model and the steric hindrance model which were applied to examine the solvation dynamics of Nile Blue and C153 in a porous sol−gel glass. The enhanced polarization field model predicts the dielectric constant of a medium confined in the pores decreases because of a preferential alignment of solvent molecules within the pores. According to this model, the polarity of a medium in a pore must be lower than that in a bulk solution phase. However, a slight red shift of the fluorescence maximum is observed in the steady-state measurements of C153 in Cal- and TMS-NAMs as listed in Table 2. This result indicates that the polarity of alcohols confined in the silica nanochannel is slightly higher than that in a bulk solution phase and that the enhanced polarization field model is not applicable to an explanation of our results. In the steric hindrance model proposed by Baumann et al.,[28] slow solvation dynamics occurs due to the sterically hindered motion of ethanol molecules at the pore surface. According to this model,[28] obvious slow solvation dynamics must be observed in Cal-NAM compared to TMS-NAM, if C153 adsorbs to the silica surface. The results shown in Table 3 conflict with the expectation of the steric hindrance model. Hence, we consider that C153 does not adsorb to the silica surface, and the steric hindrance model cannot be applicable to explain our results.

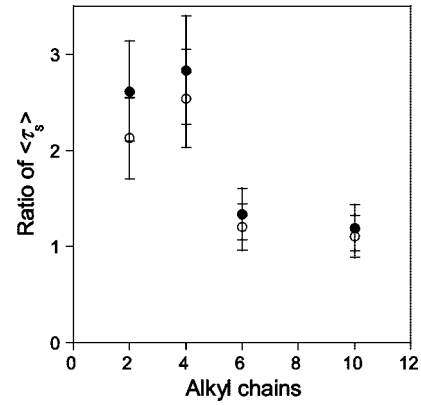

Figure 7. Ratio of the average relaxation times $\langle\tau_s\rangle_{\text{Cal-NAM}}/\langle\tau_s\rangle_{\text{bulk}}$ (open circles) and $\langle\tau_s\rangle_{\text{TMS-NAM}}/\langle\tau_s\rangle_{\text{bulk}}$ (filled circles).

From the above discussion on the contribution of water molecules and the models for porous materials, we finally consider the confinement of alcohol in the silica nanochannels as a possible cause of the slow solvation dynamics in Cal- and TMS-NAMs. As for the structure of methanol confined in the silica nanochannels, Takamuku et al.[47] studied it by large-angle X-ray scattering measurements, and they proposed a model consisting of capillary-condensed methanol molecules within a cylindrical pore. In their proposed model, methanol molecules strongly bind to the surface silanol groups of silica nanochannels (pore diameter = 2.8 or 2.1 nm) by hydrogen bonding interaction to form the surface methanol layer. A hydrophobic methyl group of the surface methanol layer interacts with a methanol molecule within a silica nanochannel by van der Waals interaction to form a head-to-head structure, and then the tail OH group can bind to another methanol molecule by hydrogen bonding interaction to form a tail-to-tail structure. These successive head-to-head and tail-to-tail structures form the methanol chains whose translational motions are strongly restricted in the silica nanochannels, while methanol molecules in bulk more loosely interact with each other because of their free three-dimensional translation motion.

Similar to the structure of the methanol chain proposed by Takamuku et al.,[47] we can consider that ethanol molecules in the silica nanochannel of Cal-NAM form the surface ethanol layer where ethanol molecules bind directly to the surface silanol groups on the wall of the silica nanochannel. Then, the head (ethyl) group of the surface ethanol layer can interact with ethanol molecules in the silica nanochannel by van der Waals interaction to form a head-to-head structure. From the successive hydrogen bonding and van der Waals interactions between ethanol molecules, a relatively rigid structure for the ethanol chain would be formed inside the silica nanochannels, which could cause the slow solvation dynamics of C153. If the surface ethanol layer is mainly responsible for the slow solvation dynamics, the average relaxation time should be larger for Cal-NAM than for TMS-NAM, because the surface ethanol layer is absent in the silica nanochannel modified with the TMS layer. However, the estimated average relaxation time of C153 is almost the same for both TMS-NAM (123 ps) and Cal-NAM (100 ps) within the experimental error, indicating that the surface ethanol layer is not the cause of the slow solvation dynamics. In the case of TMS-NAM, TMS groups are densely immobilized on the inner surface of silica nanochannels and the methyl group of the TMS layer interacts with ethanol by van der Waals interaction to form the head-to-head structure and then tail-to-tail structure similar to the case of Cal-NAM. Thus formed ethanol chains in the silica nanochannels would be the cause

of the slower solvent relaxation time observed for Cal- and TMS-NAMs compared to bulk ethanol. Since there is not much difference in the solvent relaxation times between Cal-NAM and TMS-NAM, the surface functional groups of silica nanochannels do not significantly affect the solvation dynamics.

4.2. Effect of Molecular Size of Alcohols on Solvation Dynamics. As seen in Table 3, the average solvent relaxation time $\langle\tau_s\rangle$ becomes slow in both bulk and NAMs as the length of the alkyl chain of the alcohols increases. To consider the relationship between the molecular size of alcohols and $\langle\tau_s\rangle$, the ratio of the average solvent relaxation times for Cal-NAM ($\langle\tau_s\rangle_{\text{Cal-NAM}}$) and TMS-NAM ($\langle\tau_s\rangle_{\text{TMS-NAM}}$) to that for bulk ($\langle\tau_s\rangle_{\text{bulk}}$) is plotted against the length of the alkyl chain of the alcohols in Figure 7. The ratios for both Cal- and TMS-NAMs are high for ethanol and butanol. The higher ratio means slower solvation dynamics in the silica nanochannels of Cal- and TMS-NAMs compared to bulk. Accordingly, butanol is considered to form relatively rigid alcohol chains in the silica nanochannels of Cal- and TMS-NAMs similar to the case of ethanol, which causes the slow solvation dynamics. The ratio is nearly unity for hexanol and decanol. This fact means that alcohols with long alkyl chains have a similar molecular orientation in both the silica nanochannels and bulk, and these alcohols are considered to form a loose structure inside the silica nanochannels. Compared to alcohols with longer alkyl chains, alcohols with shorter alkyl chains might easily form the alcohol chains which are assembled using the strong hydrogen bonding interaction and less strong van der Waals interaction between alcohol molecules.

In our previous study,[22] we found that tris(2,2′-bipyridyl)ruthenium ($[Ru(bpy_3)]^{2+}$) showed remarkably slow diffusivity in the silica nanochannel whose inner wall was modified by alkylsilanes compared to the diffusivity in bulk, when alcohols (methanol and ethanol) were confined in the silica nanochannel. However, the diffusivity did not become remarkably slow when aprotic solvents (acetonitrile and DMSO) were used. This result suggests that the hydrogen bonding interaction of solvent molecules confined in the silica nanochannel is significantly different from that in bulk and that the assembled structure of alcohols in the silica nanochannel could be the main cause of the slow diffusivity. In accordance with this result, slow solvation dynamics was obtained when ethanol or butanol was used as a solvent in time-resolved fluorescence measurements, suggesting that the rigidity of the assembly of alcohols (alcohol chain) is larger for shorter alcohols (ethanol and butanol) than longer alcohols (hexanol and decanol). This rigidity is well-reflected by the strong hydrogen bonding interaction compared to van der Waals interaction in the silica nanochannel. Therefore, it can be said that the hydrogen bonding interaction between solvent molecules within the silica nanochannels plays an important role in channels with a nanosized space and that the relatively rigid assembly of solvent molecules is the cause of the slow solvation dynamics and diffusivity.

5. Conclusion

Solvation dynamics of C153 in alcohols confined in silica nanochannels was studied by time-resolved fluorescence spectroscopy. It was found that the solvent relaxation times were slow in Cal- and TMS-NAMs compared to bulk when alcohols with a short alkyl chain (ethanol and butanol) were used as a solvent. In contrast, solvation dynamics in alcohols with a long alkyl chain (hexanol and decanol) did not show a significant difference between the bulk and NAM samples. As a cause of the slow solvation dynamics, formation of the alcohol chains was considered on the basis of the structure proposed from an X-ray scattering study, and it was concluded that the restricted motion of the alcohol chains in the silica nanochannel was mainly responsible for the slow solvation dynamics of C153 in ethanol and butanol confined in the silica nanochannels. Measurements of solvation dynamics could be used as a indicator of the ordering of solvent molecules confined in mesopores.

Acknowledgment. This work was supported in part by a Grant-in-Aid for Scientific Research (A), No. 17205009, from the Ministry of Education, Culture, Sports, Science and Technology, Japan, and PRESTO, Japan Science and Technology Agency (JST).

Supporting Information Available: Experimental details of the estimation of concentration of C153 within the sample membrane, additional data on steady-state fluorescence spectra, and additional data on decays of the time-correlation functions. This material is available free of charge via the Internet at http://pubs.acs.org.

References and Notes

(1) Feng, X.; Fryxell, G. E.; Wang, L.-Q.; Kim, A. Y.; Liu, J.; Kemner, K. M. *Science* **1997**, *276*, 923–926.
(2) Moreno-Tost, R.; Santamaría-González, J.; Maireles-Torres, P.; Rodríguez-Castellón, F.; Jiménez-López, A. *Catal. Lett.* **2002**, *82*, 205–212.
(3) Miyake, Y.; Yumoto, T.; Kitamura, H.; Sugimoto, T. *Phys. Chem. Chem. Phys.* **2002**, *4*, 2680–2684.
(4) Chen, H.-T.; Huh, S.; Wiench, J. W.; Pruski, M.; Lin, V. S.-Y. *J. Am. Chem. Soc.* **2005**, *127*, 13305–13311.
(5) Yiu, H. H. P.; Botting, C. H.; Botting, N. P.; Wright, P. A. *Phys. Chem. Chem. Phys.* **2001**, *3*, 2983–2985.
(6) Liu, N.; Dunphy, D. R.; Atanassov, P.; Bunge, S. D.; Chen, Z.; López, G. P.; Boyle, T. J.; Brinker, C. J. *Nano Lett.* **2004**, *4*, 551–554.
(7) Yamaguchi, A.; Uejo, F.; Yoda, T.; Uchida, T.; Tanamura, Y.; Teramae, N. *Nat. Mater.* **2004**, *3*, 337–341.
(8) Yamaguchi, A.; Teramae, N. *Anal. Sci.* **2008**, *24*, 25–30.
(9) Kageyama, K.; Tamazawa, J.; Aida, T. *Science* **1999**, *285*, 2113–2115.
(10) Han, Y.-J.; Kim, J. M.; Stucky, G. D. *Chem. Mater.* **2000**, *12*, 2068–2069.
(11) Wu, Y.; Cheng, G.; Katsov, K.; Sides, S. W.; Wang, J.; Tang, J.; Fredrickson, G. H.; Moskovits, M.; Stucky, G. D. *Nature Mater.* **2004**, *3*, 816–822.
(12) Chen, Y.; Yamaguchi, A.; Atou, T. S.; Morita, K.; Teramae, N. *Chem. Lett.* **2006**, *35*, 1352–1353.
(13) Hatton, B.; Landskron, K.; Whitnall, W.; Perovic, D.; Ozin, G. A. *Acc. Chem. Res.* **2005**, *38*, 305–312.
(14) Yoshitake, H. *New J. Chem.* **2005**, *29*, 1107–1117.
(15) Nicole, L.; Boissiére, C.; Grosso, D.; Quach, A.; Sanchez, C. *J. Mater. Chem.* **2005**, *15*, 3598–3627.
(16) Radu, D. R.; Lai, C.-Y.; Wiench, J. W.; Pruski, M.; Lin, V. S.-Y. *J. Am. Chem. Soc.* **2005**, *126*, 1640–1641.
(17) El-Safty, S. A.; Ismail, A. A.; Matsunaga, H.; Mizukami, F. *Chem. Eur. J.* **2007**, *13*, 9245–9255.
(18) Fu, W.; Yamaguchi, A.; Kaneda, H.; Teramae, N. *Chem. Commun. (Cambridge* **2008**, 853–855.
(19) Sekine, T.; Nakatani, K. *Langmuir* **2002**, *18*, 694–697.
(20) Takahashi, R.; Sato, S.; Sodesawa, T.; Ikeda, T. *Phys. Chem. Chem. Phys.* **2003**, *5*, 2476–2480.
(21) Fu, Y.; Ye, F.; Sanders, W. G.; Collinson, M. M.; Higgins, D. A. *J. Phys. Chem. B* **2006**, *110*, 9164–9170.
(22) Yamaguchi, A.; Yoda, T.; Suzuki, S.; Morita, K.; Teramae, N. *Anal. Sci.* **2006**, *21*, 1501–1507.
(23) Yamaguchi, A.; Mekawy, M. M.; Chen, Y.; Suzuki, S.; Morita, K.; Teramae, N. *J. Phys. Chem. B* **2008**, *112*, 2024–2030.
(24) Martin, C. R.; Rubinstein, I.; Bard, A. J. *J. Electroanal. Chem.* **1983**, *151*, 267–271.
(25) Coo, L. dlC.; Sadek, M.; Brownlee, R. T. C.; Cardwell, T. J.; Cattrall, R. W.; Kolev, S. D. *Anal. Chim. Acta* **1999**, *386*, 137–144.
(26) Maroncelli, M.; Fleming, G. R. *J. Chem. Phys.* **1987**, *86*, 6221–6239.
(27) Pal, S. K.; Sukul, D.; Mandal, D.; Sen, S.; Bhattacharyya, K. *J. Phys. Chem. B* **2000**, *104*, 2613–2616.

(28) Baumann, R.; Ferrante, C.; Deeg, F. W.; Bräuchle, C. *J. Chem. Phys.* **2001**, *114*, 5781–5791.
(29) Baumann, R.; Ferrante, C.; Kneuper, E.; Deeg, F. W.; Bräuchle, C. *J. Phys. Chem. A* **2003**, *107*, 2422–2430.
(30) Sahu, K.; Roy, D.; Mondal, S. K.; Halder, A.; Bhattacharyya, K. *J. Phys. Chem. B* **2004**, *108*, 11971–11975.
(31) Sen, P.; Mukherjee, S.; Patra, A.; Bhattacharyya, K. *J. Phys. Chem. B* **2005**, *109*, 3319–3323.
(32) Yamaguchi, A.; Amino, Y.; Shima, K.; Suzuki, S.; Yamashita, T.; Teramae, N. *J. Phys. Chem. B* **2006**, *110*, 3910–3916.
(33) Zhao, X. S.; Lu, G. Q.; Whittaker, A. K.; Millar, G. J.; Zhu, H. Y. *J. Phys. Chem. B* **1997**, *101*, 6525–6531.
(34) Zhao, X. S.; Lu, G. Q. *J. Phys. Chem. B* **1998**, *102*, 1556–1561.
(35) Yamashita, T.; Uchida, T.; Fukushima, T.; Teramae, N. *J. Phys. Chem. B* **2003**, *107*, 4786–4792.
(36) Siano, D. B.; Metzler, D. E. *J. Chem. Phys.* **1969**, *51*, 1856–1861.
(37) Barrett, E. P.; Joyner, L. G.; Halenda, P. P. *J. Am. Chem. Soc.* **1951**, *73*, 373–380.
(38) Kresge, C. T.; Leonowicz, M. E.; Roth, W. J.; Varturi, J. C.; Beck, J. S. *Nature* **1992**, *359*, 710–712.
(39) Lowen, W. K.; Broge, E. C. *J. Phys. Chem.* **1961**, *65*, 16–19.
(40) Zettlemoyer, A. C.; Hsing, H. H. *J. Colloid Interface Sci.* **1977**, *58*, 263–274.
(41) Sindorf, D. W.; Maciel, G. E. *J. Phys. Chem.* **1982**, *86*, 5208–5219.
(42) Fadeev, A. Y.; Eroshenko, V. A. *J. Colloid Interface Sci.* **1997**, *187*, 275–282.
(43) Ramírez, A.; Lopez, B. L.; Sierra, L. *J. Phys. Chem. B* **2003**, *107*, 9275–9280.
(44) Horng, M. L.; Gardecki, J. A.; Papazyan, A.; Maroncelli, M. *J. Phys. Chem.* **1995**, *99*, 17311–17337.
(45) Habuchi, S.; Kim, H.-B.; Kitamura, N. *Anal. Chem.* **2001**, *73*, 366–372.
(46) Yamashita, T.; Amino, Y.; Yamaguchi, A.; Teramae, N. *Chem. Lett.* **2005**, *34*, 988–989.
(47) Takamuku, T.; Maruyama, H.; Kittaka, S.; Takahara, S.; Yamaguchi, T. *J. Phys. Chem. B* **2005**, *109*, 892–899.

JP8034743